Journal of Design Against Fatigue, Vol. 4, No. 1, 2026, pp. 3-8

ORBIS ACADEMICS

Journal of Design Against Fatigue

ISSN: 2976-940X

# Mechanics of chip formation in Ultra-High Molecular Weight Polyethylene (UHMWPE)

Hassan Ghadbeigi[1,*], Luke Jones[1], Abdulrahman Hasan[1], Gemma Harling[1], Jack Rooke[2]

[1] School of Mechanical, Aerospace and Civil Engineering, University of Sheffield, Mappin Street, Sheffield, S1 3JD, UK

[2] University of Sheffield Advanced Manufacturing Research Centre, Wallis Way, Catcliffe, Rotherham, S60 5TZ, UK

* Corresponding author: Hassan Ghadbeigi; h.ghadbeigi@sheffield.ac.uk

**Article history**

Received: 7 October 2026
Revised: 29 October 2026
Accepted: 31 October 2026
Available online: 31 October 2026

***Keywords***

*Orthogonal cutting; Chip formation; UHMWPE; In situ imaging; Viscoelastic recovery; Minimum uncut chip thickness*

**Abstract**

Ultra-High Molecular Weight Polyethylene (UHMWPE) is widely used in medical and food applications but remains challenging to machine due to unstable chip formation, poor chip control, burr generation, and surface distortion. Chip formation mechanics in two grades of UHMWPE (medical-grade GUR 1050 and food-compliant PE1000) is investigated using a bespoke *in situ* orthogonal cutting rig and direct observation via high-speed imaging synchronised with force measurement. The influence of the uncut chip thickness on chip morphology and deformation behaviour was systematically examined. A gradually increasing uncut chip thickness revealed a sequence of rubbing, ploughing, mixed ploughing-shearing and shear-dominated continuous chip formation, with the crossover of the cutting and thrust forces marking the transition. The polymer grade had a profound effect on the formation of the chip within the primary and secondary deformation zones as well as the chip curvature: at similar uncut chip thickness the cutting forces of the two grades were comparable, whereas the thrust force of the medical grade was up to about 60% lower and its chip–tool contact length longer. With increasing uncut chip thickness, separation at the tool tip changed from shear to tearing ahead of the tool. The proposed methodology provides a robust platform for optimising cutting-edge geometries for improving chip control and reducing reliance on $CO_2$ cooling strategies, and for linking machining-induced surface deformation to the fatigue performance of UHMWPE components.

Doi: https://doi.org/10.62676/jdaf.2026.4.1.20

## 1. Introduction

Ultra-high molecular weight polyethylene (UHMWPE) is a high-performance thermoplastic widely used in biomedical applications due to its excellent wear resistance, chemical inertness, impact strength, and low friction [1]. The mixed amorphous and crystalline nature of this polymer together with a high degree of polymerisation give the material its remarkable toughness and ability to withstand impact [2]. The high entanglement density and crystallinity significantly affect the material's processability and response to mechanical stresses and deformation at various rates [3]. UHMWPE has demonstrated long-term biocompatibility and wear performance [1], and it has therefore been used extensively in orthopaedic implants, including hip, knee, and spinal implants, for over 1.4 million patients annually since its introduction to orthopaedics in the 1960s [4]. Owing to complex geometrical features, tight geometrical and dimensional tolerances as well as the bespoke design of each implant, machining is commonly used as the finishing process for biomedical polymers such as UHMWPE [5]. However, polymer machining presents additional complexities compared with metallic materials due to low thermal conductivity, viscoelastic behaviour and the glass transition temperature ($T_g$) [6–8]. For UHMWPE, $T_g$ lies well below room temperature, so the amorphous phase is rubbery during cutting and chip formation is governed by large-strain, rate-dependent flow, crack-assisted separation and subsequent viscoelastic recovery [9, 10]. These include unstable chip formation, burr generation, and surface distortion during machining, compromising dimensional accuracy and surface integrity [11–13]. Up to six distinct chip morphologies, strongly dependent on cutting parameters, are reported in the machining of UHMWPE, while tool sharpness further influences surface deformation and effective depth of cut as a result of elastic recovery and viscous relaxation [11]. In medical applications, UHMWPE is typically machined dry, using biocompatible coolants, or using cryogenic fluids to reduce the cutting temperature and improve surface quality [5, 14, 15]. Supercritical $CO_2$, alone or combined with minimum quantity lubrication or low-frequency vibration, has more recently been used to break chips and reduce swarf nesting and burr formation [12, 16]. Despite the significant body of research on the tribology, wear and biocompatibility of UHMWPE [17–19], its machinability, particularly the fundamental mechanics governing chip formation, remains largely unexplored; to the authors' knowledge, no direct (*in situ*) observation of the deformation zones and of tool-tip separation in UHMWPE has been reported. This limits the rational design of cutting tool geometries and the selection of machining parameters required to achieve reliable dimensional accuracy and surface integrity. Addressing this gap is critical for improving the functional performance, longevity, and manufacturability of UHMWPE components in demanding applications, not least because machined notches and rim features of UHMWPE joint components are known sites of fatigue crack initiation [20, 21].

A bespoke *in situ* orthogonal cutting rig was developed to enable a thorough analysis of chip mechanics and the effect of cutting parameters, in particular the uncut chip thickness

($a_c$), on two different grades of UHMWPE. The deformation mechanics and the variations of the chip thickness, as well as subsurface deformation, were observed and used to identify a possible approach to reduce the viscoelastic relaxation effect on the produced surfaces.

## 2. Materials and methods

### 2.1 Materials and mechanical characterisation

Compression and tensile tests were conducted on medical-grade (GUR 1050, MD) and food-compliant (PE1000, FD) UHMWPE; compression tests followed ASTM D695 and tensile tests ASTM D638. Cylindrical compression specimens (15 mm height, 10 mm diameter) were machined from MD and FD ram-extruded bars. The tests were performed at constant strain rates of $\dot{\varepsilon} = 10^{-4}$ s$^{-1}$ and $\dot{\varepsilon} = 10^{-2}$ s$^{-1}$, while the tensile tests were conducted at a displacement rate of 50 mm/min. Post-deformation dimensions of compression specimens were measured immediately after unloading and after two days to quantify viscoelastic relaxation. The resulting mechanical properties were correlated with the observed chip formation behaviour during machining.

### 2.2 In situ orthogonal cutting rig

A bespoke *in situ* orthogonal cutting rig was designed and manufactured, as shown in Fig. 1, in which rectangular samples with dimensions of 25 (l) × 15 (h) × 3 (t) mm are pushed into the cutting region using a loading frame. A sapphire glass window (Fig. 1a) was used to restrict out-of-plane deformation within the cutting region, hence satisfying the plane strain orthogonal cutting condition. Two HBM CFT/5kN piezoelectric force transducers were attached to the cutting tool holder and the plunger to measure the thrust and cutting forces, respectively. The rig has been designed with sliding tolerance in the contacting surfaces to reduce the frictional effect on the measured forces. The average frictional forces in both cutting and thrust force directions were measured to be less than 1 N. The chip formation and material deformation can be recorded through the sapphire glass window (Fig. 1b and c), while the cutting depth can be set using the tool holder mechanisms and a 1 µm resolution axial digital micrometre, and validated by the optical images. A high-speed camera (Phantom VEO 410L) equipped with a Navitar f-mount telecentric microscope lens (×25) and a synchronised high-intensity strobe light (Veritas mini CONSTELLATION 120C28) was used as the imaging system, which was triggered by the test frame displacement.

All specimens were machined from as-received ram-extruded stock and then stored under ambient conditions to ensure dimensional stabilisation prior to testing.

High-speed steel blanks were used to manufacture cutting inserts with a 10° rake and a 7° clearance angle and an edge radius of 10 microns. Several values of depth of cut were selected, and the actual removed material was measured in each case. The cutting speed was set at the maximum displacement rate of the test frame (1000 mm/min) to study the effect of material morphology and $a_c$ on the cutting forces and produced chip morphologies. The image frequency and force measurements were synchronised at 5 kHz so that the recorded chip formation incidents could be directly correlated with the corresponding measured force signal.

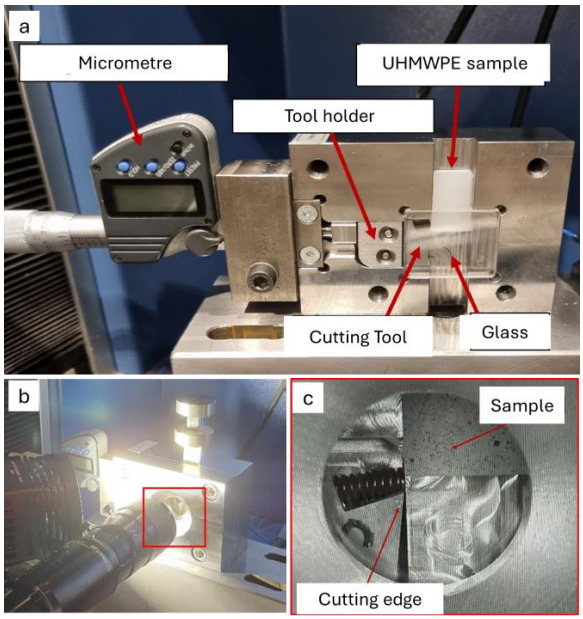



**Figure 1.** (a) Experimental setup for *in situ* orthogonal cutting, showing the (b) high-speed camera setup and (c) field of view used to analyse the deformation of the material.

Sample dimensions were measured before and after cutting to quantify the effective material removal and post-machining dimensional relaxation following chip formation. The machined sections were subsequently analysed to evaluate variations in chip thickness and material flow within the primary deformation zone (PDZ) and secondary deformation zone (SDZ).

## 3. Results

### 3.1 Tensile and compressive response of UHMWPE

Fig. 2 shows the comparison of stress–strain curves for each material under tension and compression. The MD material grade has higher stiffness as well as mechanical strength both in tension and compression, while the strain rate dependency of both grades is almost identical, as demonstrated in Fig. 2b. Such a strain rate dependency has been reported in the literature [3] and linked to the viscoelastic response of the material and locking of the polymer chains. Fig. 3 illustrates the dimensional changes of the compression specimens resulting from viscoelastic relaxation, quantified in both the axial (height) and circumferential (diameter) directions.

Although the variations of the height are almost similar in both samples, the FD grade shows a slightly lower degree of diameter variation, possibly due to the inherent microstructural properties in the crystalline phase.

### 3.2 Chip formation mechanics

The actual depth of cut (after the cutting) and associated standard deviations are shown in Fig. 4. The height of the samples was measured at five different locations prior to and after cutting using a 1 µm resolution digital micrometre, and the actual depth of cut was calculated. Sample FD1 was set up on an inclined path along which the uncut chip thickness increased gradually, to determine the onset of ploughing and shear mechanisms. Additionally, the small standard deviation of the measured values after the cut confirms the consistency of the process as well as the reliability of the developed cutting rig.

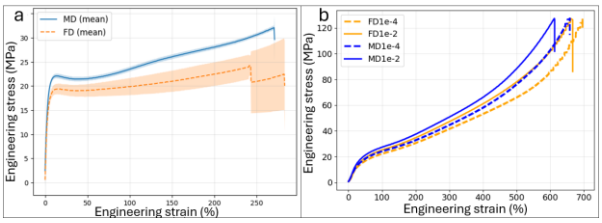



**Figure 2.** (a) Tensile stress–strain curves of MD and FD material grades, together with (b) compressive material properties at two different strain rates.

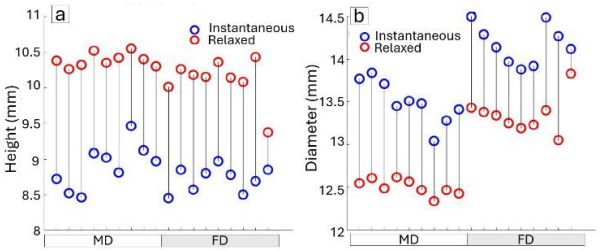



**Figure 3.** Dimensional variations after unloading for (a) height and (b) diameter of MD and FD samples. The red circles show the relaxed state, while the blue circles show the dimensions immediately after the tests.

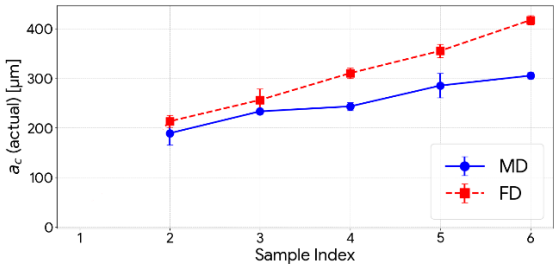



**Figure 4.** Actual $a_c$ after relaxation for FD and MD samples, together with the standard deviation of the measurements.

The measured cutting forces are shown in Fig. 5 for FD and MD samples with a similar removed layer. These indicate that at lower chip load, where less deformation is expected, both materials show similar behaviour, although higher thrust forces are observed for FD, which could be due to a slightly larger chip load. However, UHMWPE shows severe strain rate hardening, particularly at rates approaching those in machining [3], which may explain the behaviour of these two grades under these conditions.

The FD1 sample was used to investigate the evolution of the chip formation process with forces, as presented in Fig. 6 and Fig. 7. As the workpiece is pushed into the cutting zone, $F_c$ shows a sudden increase (1 in Fig. 6) due to the initial contact. The cutting tool rubs over the surface (Fig. 7b), resulting in slight variations in the forces, until the instantaneous uncut chip thickness and the material relaxation balance initiate the shear mechanism (2 in Fig. 6). At this point the minimum uncut chip thickness for the specific tool geometry is reached. The stored strain energy at this point is suddenly released (3 in Fig. 6) by the shearing deformation and initiation of chip formation. Although some chips are observed at the cutting edge (Fig. 7c), ploughing is still the dominant mechanism up to point 4 (Fig. 6), where the cutting and thrust forces are equal. Thereafter, a continuous chip is formed, as indicated by the increase in the cutting and thrust forces, the slope of which can be used to calculate the cutting force coefficients for the prediction of the forces.

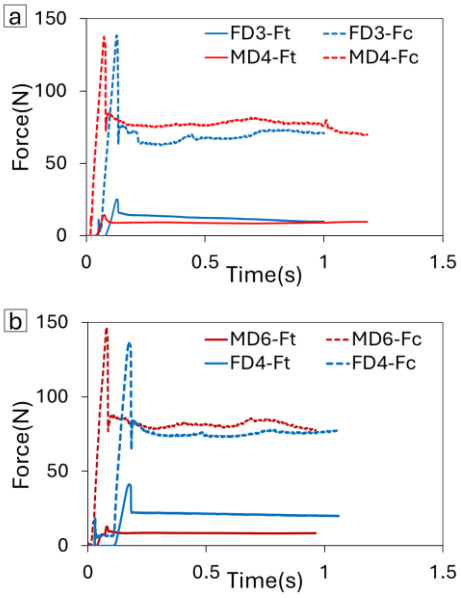



**Figure 5.** Comparison of cutting ($F_c$) and thrust ($F_t$) forces in FD and MD samples with similar $a_c$(actual): (a) FD3 and MD4; (b) MD6 and FD4, showing a markedly lower thrust force for MD, with the difference increasing with $a_c$.

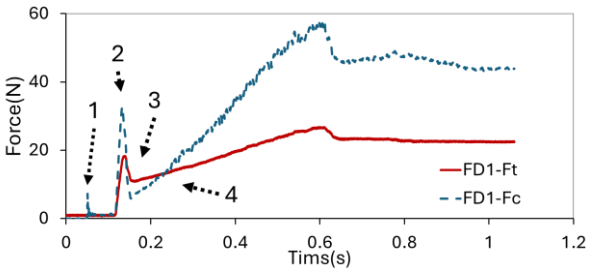



**Figure 6.** Evolution of machining forces in FD1 under a gradually increasing depth of cut, indicating the onset of ploughing, mixed and shear-dominant chip formation; events 1–4 correspond to the frames in Fig. 7.

The material deformation in the tertiary deformation zone starts at the early stages of chip formation, where ploughing is the dominant chip formation mechanism, as shown by the arrows in Fig. 7. However, it was observed that the size of the affected region does not change once steady-state chip formation is reached.

Fig. 8 demonstrates the primary deformation zone region for both materials when cutting with a small (FD2/MD4) and a larger (FD6/MD6) depth of cut. The area in the vicinity of the tool tip is indicated by the arrows, showing that as the depth of cut, and hence the local shear stress, increases, a crack is formed ahead of the tool. Therefore, the separation is controlled by ductile tearing of the material ahead of the tool under mixed-mode (I/II) loading [22, 23]. This explains the almost identical cutting forces observed for both materials (Fig. 5), as the shear strength and fracture toughness of the materials are of the same order of magnitude.

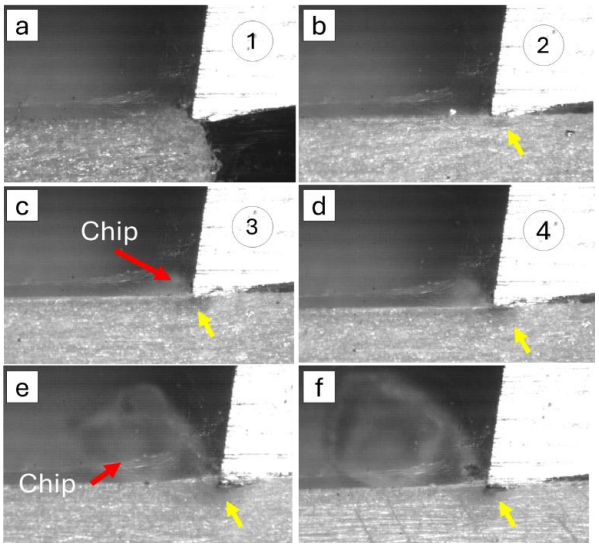



**Figure 7.** Chip formation evolution in the FD1 sample from (a) zero depth of cut to (b) ploughing and (c–f) shear-dominant chip formation leading to the continuous chip; circled numbers correspond to events 1–4 in Fig. 6. The yellow arrows show the development of tertiary deformation, where the cutting tool is pushed back by the material; red arrows indicate the chip.

However, the significant reduction of the thrust force in the MD grade could be linked to its local properties, largely its amorphous structure and viscoplasticity. This increases the material spring-back after deformation, which occurs due to the strain hardening and rate-sensitive properties. This is shown in Fig. 8, in which shear bands are clearly visible within the chip section of FD samples, indicating a higher degree of crystallinity as well as deformation due to the frictional stresses on the rake face.

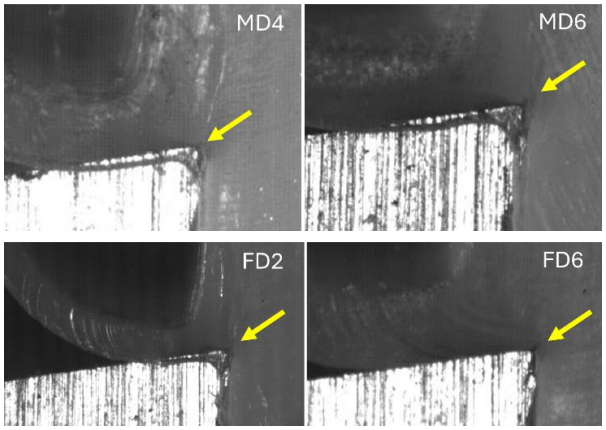



**Figure 8.** Primary deformation zone in MD and FD samples, showing a transition from shear to tearing at the tool tip with increasing $a_c$ (arrows).

The chip-tool contact length is longer in MD samples cut with similar $a_c$, MD6 (722 µm) vs. FD4 (614 µm), which is linked to the chip curvature, as shown in Fig. 9. The larger curvature of the chip results in more entanglement around the cutting tool and requires further attention in finishing operations [15].

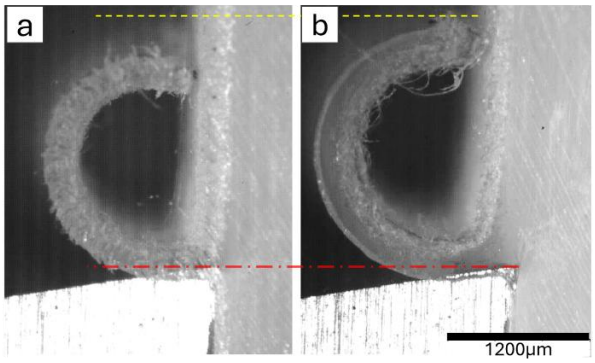



**Figure 9.** Chip curl and chip–tool contact in MD and FD samples cut at similar $a_c$ (MD6 and FD4, $a_c \approx 0.31$ mm).

## 4. Discussion

### 4.1 Ploughing-to-shear transition and minimum uncut chip thickness

The force signature of the inclined-path test (Fig. 6) provides an operational definition of the minimum uncut chip thickness: below it, the edge rubs and ploughs the surface and the thrust force exceeds the cutting force, whereas the crossover $F_c = F_t$ (event 4) marks the onset of shear-dominated chip formation. Force-ratio and specific-energy criteria of this kind are widely used to identify the minimum uncut chip thickness in precision and micro-machining [24]; the present results show that the same concept applies to a viscoelastic polymer, in which the effective chip thickness is further reduced by elastic recovery and viscous relaxation [11]. Because the minimum uncut chip thickness scales with the cutting-edge radius, and tool sharpness is known to affect the forces measured when cutting polymers [25], expressing the transition thickness relative to the measured edge radius would make the result transferable to tool design.

### 4.2 Separation at the tool tip and grade-dependent forces

The change from shear-dominated flow to crack-assisted separation ahead of the tool with increasing $a_c$ (Fig. 8) supports a fracture-mechanics view of cutting, in which the cutting force comprises the plastic work in the primary zone, the frictional work on the rake face and the work of separation that creates the new surfaces [22, 26]. For polymers, the separation work can be extracted from the intercept of the cutting force per unit width plotted against $a_c$, after correction for friction [26, 27], and it has been shown to behave as a mixed-mode toughness [23]. Applying this analysis to the MD and FD data would establish whether the similar cutting forces of the two grades (Fig. 5) reflect a similar separation toughness, as suggested in Section 3.2.

The markedly lower thrust force of MD at similar $a_c$ is consistent with lower rake-face friction. Resolving the forces in Fig. 5b onto a rake face inclined at 10° gives an apparent friction coefficient of about 0.28 for MD6 and 0.48 for FD4, and mean rake-face shear stresses of roughly 10 MPa and 18 MPa over the measured contact lengths of 722 µm and 614 µm, respectively; these are upper-bound estimates because the edge (ploughing) forces have not been separated. Differences in chip curl and shear banding between polyethylenes of different structure have also been reported by Xiao and Zhang, who related inward curl to deformation in the secondary zone and outward curl to shear

banding in the primary zone [10]. Measuring the crystallinity of both grades, for example by differential scanning calorimetry, would allow these differences to be attributed to polymer structure.

### 4.3 Strain rate and temperature: relevance to production machining

The tests were performed at 1 m/min, two to three orders of magnitude below the cutting speeds used to turn and mill UHMWPE components (200–400 m/min in turning [15] and up to about 970 m/min in high-speed milling [16]). Taking a primary shear zone thickness of 0.1–0.3 mm, the shear strain rate in the present tests is estimated at $10^1$–$10^2$ $s^{-1}$, already four to six orders of magnitude above the rates of the compression tests. Compression data for bulk UHMWPE from $10^{-4}$ to 2600 $s^{-1}$ and from −75 °C to 100 °C [3] could therefore be used to estimate the flow stress in the primary zone. At 1 m/min the process is essentially isothermal, which isolates the mechanical response of the two grades; at production speeds, frictional and plastic heating combined with the low thermal conductivity of UHMWPE soften the material, which is the motivation for cryogenic and $CO_2$-based cooling [5, 12, 15, 16]. Tool geometries that shorten the ploughing regime and promote early, stable chip separation offer a route to better chip control with less reliance on such cooling.

### 4.4 Implications for surface integrity and fatigue of UHMWPE components

For load-bearing UHMWPE components, the machined surface is not only a dimensional feature but also a potential site of fatigue crack initiation. Notches built into acetabular liners and tibial posts promote fatigue crack initiation [20], and retrieval studies of cross-linked acetabular liners have found fatigue cracks initiating at stress concentrations, including the root of rim notches, which are regarded as precursors to rim fracture [21, 28]. The fatigue and fracture resistance of UHMWPE is, in turn, sensitive to its microstructure and processing [29]. The present observations identify three machining-related features that may affect this behaviour: (i) the tertiary (flank) deformation zone, which forms during ploughing and persists at constant size during steady-state cutting (Fig. 7); (ii) crack-assisted tearing ahead of the tool at larger $a_c$ (Fig. 8), which may leave a torn rather than a sheared surface; and (iii) time-dependent recovery, which changes the final geometry after machining (Figs. 3 and 4). In metals, machining-induced surface topography, subsurface deformation and residual stresses are well-established controls on fatigue life [30]. Establishing equivalent links for UHMWPE, for example through notch fatigue tests on specimens machined in the ploughing- and shear-dominated regimes, would connect the chip formation mechanics reported here to design against fatigue.

### 4.5 Limitations

The results were obtained at a single, low cutting speed with one tool geometry and a limited number of samples per $a_c$ level; the imaged face is in contact with the sapphire window and may not fully represent the flow at mid-thickness; and the crystallinity of the two grades was not measured. Extending the tests to higher speeds, repeated cuts and microstructural characterisation would allow the mechanisms identified here to be generalised.

## 5. Conclusions

The mechanics of chip formation in medical-grade (GUR 1050) and food-compliant (PE1000) UHMWPE were studied using a bespoke *in situ* orthogonal cutting rig with synchronised force measurement and high-speed imaging. The main conclusions are as follows.

(1) Under a gradually increasing uncut chip thickness, chip formation progressed from rubbing to ploughing, mixed ploughing–shearing and shear-dominated continuous chip formation. The crossover of the cutting and thrust forces provides an operational marker of the minimum uncut chip thickness for a given tool.

(2) At similar uncut chip thickness, the cutting forces of the two grades were comparable, whereas the thrust force of the medical grade was markedly lower (by about 60% at $a_c \approx 0.31$ mm), with a longer chip–tool contact length and a more strongly curled chip, consistent with lower rake-face friction.

(3) With increasing uncut chip thickness, material separation at the tool tip changed from shear-dominated flow to crack-assisted tearing ahead of the tool, indicating that the work of separation contributes to the cutting energy of UHMWPE.

(4) Both grades showed substantial viscoelastic recovery after compression, and deformation of the machined surface (tertiary zone) initiated during ploughing and remained of constant extent during steady-state cutting. These features define the machining-affected surface layer that is relevant to the dimensional accuracy and fatigue performance of UHMWPE components.

## Competing interests

The authors declare that they have no known competing financial interests or personal relationships that could have appeared to influence the work reported in this paper.

## Author contributions

**Hassan Ghadbeigi:** Conceptualization, Methodology, Formal analysis, Visualization, Resources, Supervision, Writing- original draft, Writing - review & editing.

**Luke Jones:** Investigation, Formal analysis.

**Abdulrahman Hasan:** Investigation, Formal analysis.

**Gemma Harling:** Investigation, Formal analysis

**Jack Rooke:** Resources.

## References

[1] M. C. Sobieraj, C. M. Rimnac, "Ultra high molecular weight polyethylene: mechanics, morphology, and clinical behavior," *Journal of the Mechanical Behavior of Biomedical Materials*, vol. 2, no. 5, pp. 433–443, 2009, https://doi.org/10.1016/j.jmbbm.2008.12.006.

[2] A. G. Fisch, N. da Silveira Jr, N. S. Cardozo, A. R. Secchi, J. H. dos Santos, J. B. Soares, "Direct production of ultra-high molecular weight polyethylene with oriented crystalline microstructures," *Journal of Molecular Catalysis A: Chemical*, vol. 366, pp. 74–83, 2013.

[3] E. N. Brown, R. B. Willms, G. T. Gray, P. J. Rae, C. M. Cady, K. S. Vecchio, J. Flowers, M. Y. Martinez, "Influence of molecular conformation on the constitutive response of polyethylene: a comparison of HDPE, UHMWPE, and PEX," *Experimental Mechanics*, vol. 47, no. 3, pp. 381–393, 2007, https://doi.org/10.1007/s11340-007-9045-9.

[4] M. K. Musib, "A review of the history and role of UHMWPE as a component in total joint replacements," *International Journal of Biological Engineering*, vol. 1, no. 1, pp. 6–10, 2012.

[5] Y. Kakinuma, S. Kidani, T. Aoyama, "Ultra-precision cryogenic machining of viscoelastic polymers," *CIRP Annals*, vol. 61, no. 1, pp. 79–82, 2012, https://doi.org/10.1016/j.cirp.2012.03.039.

[6] M. Píška, K. Urbancová, "Advanced machining of joint implant UHMWPE inserts," *Machines*, vol. 10, no. 11, Art. no. 1008, 2022, https://doi.org/10.3390/machines10111008.

[7] D. D. da Costa, H. L. Corrêa, C. J. Rebeyka, S. F. Zawadzki, "UHMWPE molecular structure analysis after turning operations and machinability with a standard off-the-shelf carbide tool," *Engineering Research Express*, vol. 1, no. 2, Art. no. 025039, 2019.

[8] D. Axinte, Y. Guo, Z. Liao, A. J. Shih, R. M'Saoubi, N. Sugita, "Machining of biocompatible materials — recent advances," *CIRP Annals*, vol. 68, no. 2, pp. 629–652, 2019, https://doi.org/10.1016/j.cirp.2019.05.003.

[9] J. W. Carr, C. Feger, "Ultraprecision machining of polymers," *Precision Engineering*, vol. 15, no. 4, pp. 221–237, 1993, https://doi.org/10.1016/0141-6359(93)90105-J.

[10] K. Q. Xiao, L. C. Zhang, "The role of viscous deformation in the machining of polymers," *International Journal of Mechanical Sciences*, vol. 44, pp. 2317–2336, 2002, https://doi.org/10.1016/S0020-7403(02)00178-9.

[11] B. Aldwell, R. Hanley, G. E. O'Donnell, "Characterising the machining of biomedical grade polymers," *Proceedings of the Institution of Mechanical Engineers, Part B: Journal of Engineering Manufacture*, vol. 228, no. 10, pp. 1237–1251, 2014.

[12] J. Rooke, R. Bonnell, E. Pickford, A. Brown, D. Curtis, "Application of low frequency vibration to the turning of ultra-high molecular weight polyethylene," *Advanced Manufacturing: Polymer & Composites Science*, vol. 11, no. 1, Art. no. 2449631, 2025, https://doi.org/10.1080/20550340.2025.2449631.

[13] B. Denkena, K. M. Heide, M.-E. Eggers, C. K. Emonde, C. Hurschler, "Analysis on micro-milling of UHMWPE for the integration of radiopaque markers on the surface of TKA inlays," *Production Engineering*, vol. 20, no. 1, Art. no. 9, 2026, https://doi.org/10.1007/s11740-025-01401-7.

[14] R. Bertolini, A. Ghiotti, S. Bruschi, "Machinability of polyamide 6 under cryogenic cooling conditions," *Procedia Manufacturing*, vol. 48, pp. 419–427, 2020.

[15] R. Bertolini, A. Ghiotti, S. Bruschi, "Cryogenic machining to enhance surface finish of a biomedical grade ultra-high-molecular weight polyethylene," in *Proceedings of ESAFORM 2021: 24th International Conference on Material Forming*, Liège, Belgium, 2021, https://doi.org/10.25518/esaform21.3749.

[16] A. Siahsarani, S. Fattahi, A. Alinaghizadeh, B. Azarhoushang, R. Bösinger, "Data-driven optimization of processing parameters and cooling strategies in UHMWPE high speed milling through multi-criteria decision making using PCA and Pareto-based evolutionary algorithms," *International Journal of Precision Engineering and Manufacturing-Green Technology*, vol. 13, no. 3, pp. 1099–1114, 2026, https://doi.org/10.1007/s40684-025-00836-8.

[17] F. P. Zaribaf, "Medical-grade ultra-high molecular weight polyethylene: past, current and future," *Materials Science and Technology*, vol. 34, no. 16, pp. 1940–1953, 2018.

[18] M. Hussain, R. A. Naqvi, N. Abbas, S. M. Khan, S. Nawaz, A. Hussain, N. Zahra, M. W. Khalid, "Ultra-high-molecular-weight-polyethylene (UHMWPE) as a promising polymer material for biomedical applications: a concise review," *Polymers*, vol. 12, no. 2, Art. no. 323, 2020, https://doi.org/10.3390/polym12020323.

[19] M. Hasegawa, S. Tone, Y. Naito, A. Sudo, "Ultra-high-molecular-weight polyethylene in hip and knee arthroplasties," *Materials*, vol. 16, no. 6, Art. no. 2140, 2023, https://doi.org/10.3390/ma16062140.

[20] F. Ansari, B. Gludovatz, A. Kozak, R. O. Ritchie, L. A. Pruitt, "Notch fatigue of ultrahigh molecular weight polyethylene (UHMWPE) used in total joint replacements," *Journal of the Mechanical Behavior of Biomedical Materials*, vol. 60, pp. 267–279, 2016, https://doi.org/10.1016/j.jmbbm.2016.02.014.

[21] J. Furmanski, M. J. Kraay, C. M. Rimnac, "Crack initiation in retrieved cross-linked highly cross-linked ultrahigh-molecular-weight polyethylene acetabular liners: an investigation of 9 cases," *The Journal of Arthroplasty*, vol. 26, no. 5, pp. 796–801, 2011, https://doi.org/10.1016/j.arth.2010.07.016.

[22] A. G. Atkins, "Modelling metal cutting using modern ductile fracture mechanics: quantitative explanations for some longstanding problems," *International Journal of Mechanical Sciences*, vol. 45, no. 2, pp. 373–396, 2003, https://doi.org/10.1016/S0020-7403(03)00040-7.

[23] D. J. Wyeth, A. G. Atkins, "Mixed mode fracture toughness as a separation parameter when cutting polymers," *Engineering Fracture Mechanics*, vol. 76, no. 18, pp. 2690–2697, 2009, https://doi.org/10.1016/j.engfracmech.2009.07.023.

[24] S. Wojciechowski, "Estimation of minimum uncut chip thickness during precision and micro-machining processes of various materials—a critical review," *Materials*, vol. 15, no. 1, Art. no. 59, 2022, https://doi.org/10.3390/ma15010059.

[25] B. R. K. Blackman, T. R. Hoult, Y. Patel, J. G. Williams, "Tool sharpness as a factor in machining tests to determine toughness," *Engineering Fracture Mechanics*, vol. 101, pp. 47–58, 2013, https://doi.org/10.1016/j.engfracmech.2012.09.020.

[26] J. G. Williams, Y. Patel, B. R. K. Blackman, "A fracture mechanics analysis of cutting and machining," *Engineering Fracture Mechanics*, vol. 77, no. 2, pp. 293–308, 2010, https://doi.org/10.1016/j.engfracmech.2009.06.011.

[27] Y. Patel, B. R. K. Blackman, J. G. Williams, "Determining fracture toughness from cutting tests on polymers," *Engineering Fracture Mechanics*, vol. 76, no. 18, pp. 2711–2730, 2009.

[28] J. Furmanski, M. Anderson, S. Bal, A. S. Greenwald, D. Halley, B. Penenberg, M. Ries, L. Pruitt, "Clinical fracture of cross-linked UHMWPE acetabular liners," *Biomaterials*, vol. 30, no. 29, pp. 5572–5582, 2009, https://doi.org/10.1016/j.biomaterials.2009.07.013.

[29] L. A. Pruitt, "Deformation, yielding, fracture and fatigue behaviour of conventional and highly cross-linked ultra high molecular weight polyethylene," *Biomaterials*, vol. 26, no. 8, pp. 905–915, 2005, https://doi.org/10.1016/j.biomaterials.2004.03.022.

[30] D. Novovic, R. C. Dewes, D. K. Aspinwall, W. Voice, P. Bowen, "The effect of machined surface topography and integrity on fatigue life," *International Journal of Machine Tools and Manufacture*, vol. 44, no. 2–3, pp. 125–134, 2004, https://doi.org/10.1016/j.ijmachtools.2003.10.018.

**Copyright:** © 2026 by the author(s). Published by Orbis Academics, Devon, UK. This is an open access article distributed under the terms and conditions of the Creative Commons Attribution (CC BY) License. (https://creativecommons.org/licenses/by/4.0/).